OPEN ACCESS



JWST Directly Images Giant Planet Candidates Around Two Metal-polluted White Dwarf Stars

Susan E. Mullally , John Debes , Misty Cracraft , Fergal Mullally , Sabrina Poulsen , Loic Albert , Loic Albert , Katherine Thibault , William T. Reach , J. J. Hermes , Thomas Barclay , Mukremin Kilic , and Elisa V. Quintana , Space Telescope Science Institute, 3700 San Martin Drive, Baltimore, MD 21218, USA; smullally stsci.edu

AURA for the European Space Agency (ESA), Space Telescope Science Institute, 3700 San Martin Drive, Baltimore, MD 21218, USA

Constellation, 1310 Point Street, Baltimore, MD 21231, USA

Homer L. Dodge Department of Physics and Astronomy, University of Oklahoma, 440 W. Brooks Street, Norman, OK 73019, USA

Institut Trottier de recherche sur les exoplanètes and Département de Physique, Université de Montréal, 1375 Avenue Thérèse-Lavoie-Roux, Montréal, QC, H2V 0B3, Canada

Abstract

We report the discovery of two directly imaged, giant planet candidates orbiting the metal-rich, hydrogen atmosphere white dwarfs WD 1202–232 and WD 2105–82. JWST's Mid-Infrared Instrument (MIRI) data on these two stars show a nearby resolved source at a projected separation of 11.47 and 34.62 au, respectively. Assuming the planets formed at the same time as their host stars, with total ages of 5.3 and 1.6 Gyr, the MIRI photometry is consistent with giant planets with masses $\approx 1-7\,M_{\rm Jup}$. The probability of both candidates being false positives due to red background sources is approximately 1 in 3000. If confirmed, these would be the first directly imaged planets that are similar in both age and separation to the giant planets in our own solar system, and they would demonstrate that widely separated giant planets like Jupiter survive stellar evolution. Giant planet perturbers are widely used to explain the tidal disruption of asteroids around metal-polluted white dwarfs. Confirmation of these two planet candidates with future MIRI imaging would provide evidence that directly links giant planets to metal pollution in white dwarf stars.

Unified Astronomy Thesaurus concepts: DA stars (348); Exoplanet astronomy (486); Exoplanet detection methods (489); James Webb Space Telescope (2291)

1. Introduction

While some of the first exoplanets ever discovered were found orbiting evolved stars (Wolszczan & Frail 1992), only a small fraction of the more than 5000 confirmed exoplanets are known to orbit non-main-sequence stars. As a result, we have few observational constraints on what happens to planetary systems in the late stages of stellar evolution. Most stars, and all low-mass stars, end their lives as white dwarf stars (WDs; Fontaine et al. 2001). Finding exoplanets around these remnants can teach us about the fate of the planets in our own solar system.

Theory suggests that exoplanets should exist around WDs. Outer planets (those in orbits beyond approximately the asteroid belt) should survive unscathed, while planets inward of ~ 1 au should be engulfed or tidally disrupted during the red giant phase (Soker et al. 1984; Mustill & Villaver 2012). Those that survive are expected to migrate outward due to the mass loss of the star. Radial velocity surveys of evolved giant-branch stars currently undergoing mass loss have found no difference in planet occurrence rates for giant planets compared to main-sequence stars (Wolthoff et al. 2022).

Despite several surveys of WDs using various techniques to find surviving massive giant planets (e.g., Burleigh et al. 2002, 2008; Debes et al. 2005a; Farihi et al. 2008; Hogan et al. 2009;

Original content from this work may be used under the terms of the Creative Commons Attribution 4.0 licence. Any further distribution of this work must maintain attribution to the author(s) and the title of the work, journal citation and DOI.

van Sluijs & Van Eylen 2018; Brandner et al. 2021), only a few planetary mass objects have been found orbiting WDs. Recent examples of giant planets found orbiting single WDs include one found via microlensing (MOA-2010-BLG-477Lb; Blackman et al. 2021) and another found transiting with a short orbital period (WD 1856+534 b; Vanderburg et al. 2020). Also, Luhman et al. (2012), using Spitzer IRAC, succeeded in finding a cool, low-mass, brown dwarf at a separation of 2500 au with common proper motion to a WD and Gänsicke et al. (2019) found evidence of a giant planet accreting onto a WD.

Substantial evidence for planets around WDs comes from the presence of photospheric metals in 25%-50% of isolated, hydrogen-atmosphere WDs (Koester et al. 2014). These metalrich WDs must be actively accreting since the strong gravitational field pulls heavier elements out of the atmosphere on timescales as short as a few days (Koester 2009) leaving a chemically pure exterior of hydrogen. Relic planetary systems are the favored theory for the source of the accreted material (Alcock et al. 1986; Jura 2003). In this scenario, planets that survive the red giant phase occasionally perturb the orbits of asteroids and comets (Debes et al. 2012), which then fall in toward the WD. When these bodies pass inside the Roche limit of the star, they disintegrate into a cloud of dust and gas, which then accretes onto the star. Support for this theory comes from the similarity between the chemical composition of the accreted material and the composition of the bulk Earth (e.g., Melis et al. 2011; Xu et al. 2019; Trierweiler et al. 2023).

JWST's infrared capabilities offer a unique opportunity to directly image Jupiter mass planets orbiting nearby WDs. The

⁶ Stratospheric Observatory for Infrared Astronomy, Universities Space Research Association, NASA Ames Research Center, Moffett Field, CA 94035, USA Department of Astronomy, Boston University, 725 Commonwealth Avenue, Boston, MA 02215, USA NASA Goddard Space Flight Center, 8800 Greenbelt Road, Greenbelt, MD 20771, USA Received 2023 December 5; revised 2024 January 11; accepted 2024 January 23; published 2024 February 15

Table 1
Atmospheric Parameters for WD 1202–232 and WD 2105–82

Name	K _{mag} (Vega)	T _{eff} (K)	log g (cgs)	Dist. (pc)	$M_{ m WD} \ ({ m M}_{\odot})$	$M_{ m MS} \ ({ m M}_{\odot})$	Total Age (Gyr)
WD 1202-232	12.3	8760 ± 130	8.01 ± 0.05	10.43	$0.60^{+0.03}_{-0.02}$	$1.3^{+0.4}_{-0.3}$	5.3 ^{+5.0} _{-2.5}
WD 2105-82	13.5	9890 ± 170	8.22 ± 0.08	16.18	$0.70^{+0.06}_{-0.05}$	$2.5^{+0.6}_{-0.7}$	$1.6^{+0.8}_{-0.2}$

Note. Ages and masses inferred using wdwarfdate (Kiman 2022); distances from Gaia Collaboration et al. (2023). Atmospheric parameters for WD 1202–232 are based on the optical spectroscopy of Gianninas et al. (2011) with the 3D corrections of Tremblay et al. (2013), and for WD 2105–82 are based on the radiative-atmosphere, optical spectroscopic fits of Gentile Fusillo et al. (2018).

contrast between a cool planet and the small, hot WD is favorable, often better than 1:200. Taking advantage of JWST's superb resolution, it is possible to directly image a planet at only a few astronomical units from nearby WDs without the use of a coronagraph. Additionally, because nearby WDs are typically several billion years old, planets found would be similar in age to those in our own solar system. A recent paper by Poulsen et al. (2023) demonstrates the exoplanet mass limits that can be achieved with JWST's MIRI imaging of both unresolved and resolved companions. Those observations are the deepest search to date for a WD; the 15 μ m band would have been able to detect a 3 Gyr, 0.34 $M_{\rm Jup}$ planet. That mass limit is \approx 20 times better than that achieved with previous Spitzer or Hubble observations of WDs (Debes et al. 2005b; Mullally et al. 2007).

In this Letter, we report evidence of directly imaged giant planets orbiting two nearby, metal-polluted WDs. Multiband mid-infrared imaging of each WD shows evidence of a red point source around each target that is consistent with a giant planet. We discuss potential sources of false positives and describe the observations required to confirm the candidates. We conclude by discussing the implications of this discovery in regard to validating the theory that metal pollution on WDs is caused by giant planets.

2. Methods

2.1. White Dwarf Star Properties

WD 1202–232 (LP 852-7) and WD 2105–82 (GJ820.1) were two of four stars chosen for deep MIRI observations as part of the General Observer Program 1911 (Mullally et al. 2021). The four target stars (the other two were WD 1620-391 and WD 2149+02) were chosen as they were isolated, had metals in their atmospheres (Subasavage et al. 2017), and were either young or nearby to improve MIRI's sensitivity to giant exoplanets. Assuming any planet orbiting the WD formed at the same time as the star, younger stars will have warmer, brighter planets in the mid-infrared. Both stars have hydrogen atmospheres (type DA) and their metal lines indicate that material is actively accreting onto their surfaces. WD 2105–82 is also known to be magnetic with a polar field of roughly 50 kG (Landstreet et al. 2012).

Table 1 provides recent measurements of effective temperature, gravity, distance, and brightness for each star. This information is used to derive the age of the star, a key piece of information to determine the expected brightness of any planet found in the system. The total age is made up of the cooling age plus the main-sequence age. We calculate the total age using the wdwarfdate (Kiman 2022) software, and rely on the cooling models of Bédard et al. (2020), the initial-to-final mass relation of Cummings et al. (2018), and the stellar evolutionary models of Choi et al. (2016). WD 1202–232 has an initial mass of

1.3 M_{\odot} and a cooling age of 0.90 Gyr, resulting in a total age of $5.3^{+5.0}_{-2.5}$ Gyr. WD 2105–82 has an initial mass of 2.5 M_{\odot} and a cooling age of 0.83 Gyr, resulting in a total age of $1.6^{+0.8}_{-0.2}$ Gyr. The relatively large errors in the age measurement for WD 1202 –232 are due to relatively large systematic uncertainties for the progenitor mass estimates for WDs with masses below 0.63 M_{\odot} (Heintz et al. 2022).

2.2. MIRI Imaging

JWST targeted the WDs with the mid-infrared instrument (MIRI) in imaging mode with four different broadband filters: F560W, F770W, F1500W, and F2100W. The observations' exposures were designed to make it possible to detect at least a $1\,M_{\rm Jup}$ planet orbiting the WD. The observations of WD 1202 -232 were taken on 2023 February 9 and the observations of WD 2105-82 were taken on 2023 April 21. Each image was composed of many exposures dithered using the cycling dither pattern with the FASTR1 readout pattern. The exposure times for the four filters for WD 1202-232 from shortest to longest wavelength were 255.3, 277.5, 8413.9, and 1309.8 s. For WD 2105-82 the four filter exposure times were 233.1, 233.1, 12088.1, and 6016.3 s.

The images were processed using build 9.2 (data processing software version 2022_5c and calibration software version of 1.11.4) of the JWST Calibration pipeline⁹ starting from the uncal files, using a CRDS context from jwst_1130.pmap and CRDS version of 11.17.6. Each set of images was processed through stages one and two of the imaging pipeline using mostly default parameters. After the stage two pipeline was run, a mean background image was created for each filter and subtracted from each cal file. Lastly, the level three imaging pipeline was run on the background-subtracted files and combined with the resample kernel set to "Gaussian" and the outlier detection "scale" values being set to (1.0 and 0.8), but using the standard parameter reference files for all other parameter settings. These background-subtracted cal and i2d files were used for all subsequent analyses. All data can be found at doi:10.17909/kak5-tx90.

2.3. Point-spread Function Subtraction and Aperture Photometry of the Candidates

To search for close companions to our targets, we performed reference differential imaging. After some experimentation, we found that the best reference point-spread functions (PSFs) for our program came from the other WDs; good PSF subtraction with MIRI imaging seems to require both a similar color as the

https://jwst-docs.stsci.edu/jwst-science-calibration-pipeline-overview/jwst-operations-pipeline-build-information/jwst-operations-pipeline-build-9-2-release-notes

Table 2
Photometric Measurements in the Four JWST Bands of the WDs and the Candidate Companion to the WDs

Object	F560W (μJy)	F770W (μ J y)	F1500W (μJy)	F2100W (μJy)
WD 1202-232	1208 ± 36	699 ± 21	181 ± 5	105 ± 3
WD 1202-232 b	1.6 ± 0.1	1.5 ± 0.1	3.0 ± 0.1	11.9 ± 0.6
WD 2105-82	428 ± 13	229 ± 7	68 ± 2	35 ± 1
WD 2105-82 b	0.7 ± 0.2	0.7 ± 0.2	2.2 ± 0.1	5.5 ± 0.3

Note. Error bars all include a 3% error bar from photometric calibrations. This is the dominant error for the WD photometry.

target and similar placement on the detector. This is most noticeable for F560W and F770W, where we also need a good removal of the cruciform feature. We judge the best PSF in each case to be the one that leaves the smallest visible residuals and is hitting the noise floor as close as possible to the location of the star. We only found a point source near (within \approx 3" of) the target star for WD 1202–232 and WD 2105–82. The other two stars show no evidence of a candidate (for WD2149+021 see Poulsen et al. 2023).

For WD 1202–232, we constructed average PSFs for each filter and masked out background sources. For F560W we found the best results with a combination of WD 1620–391 and WD 2149+021 PSFs (Mullally et al. 2021; Poulsen et al. 2023). At F770W, only WD 1620-391 provided the best subtraction, and for F1500W and F2100W a combination of the PSFs for WD 1620–391, WD 2149+021, and WD 2105–82 were satisfactory. We used the same procedure for WD 2105–82. In this case, we made use of the PSFs for the other three WDs since the companion is well separated; however, we obtained a better subtraction for F1500W by excluding WD 1202–232. Even without PSF subtraction, the two candidates are easily discernible, and the PSF subtraction does not reveal any other candidates closer than those detected.

In order to determine the flux of the candidates in each filter, we performed aperture photometry. First, to get a high-quality absolute flux measurement of the star in each filter, we used aperture photometry on the target star first using the techniques described by Poulsen et al. (2023). To maximize signal-to-noise on the candidates, we then calculated the photometry in an aperture equivalent to half the PSF FWHM in each filter and performed the same measurement on the unsubtracted star's PSF. We then took the ratio between the candidate and star's photometry calculated using this small aperture. We then multiplied this ratio by the star's absolute flux measurement in each filter. The extracted photometry for each filter are reported in Table 2.

3. Results

The goal of this study is to identify candidate substellar companions to the WDs. We expect these to appear as point sources that increase in brightness at longer wavelengths. The expected shape of the spectral energy distribution (SED) of old, cool giant planets in these broadband filters is not well known; models show that temperature, composition, and cloud cover can all impact these bands. Here we discuss the evidence for directly imaged planet candidates in the MIRI observations. We compare the four band SEDs of both candidates with planet models and constrain the mass of the planet assuming the

observed sources lie at the distance of the star and have an age matching that of the WD. We also examine whether the target is a point source by looking at the Gaussian shape of the center of the source and by subtracting a PSF from the companion and looking at the residuals. Finally, we explore the overall likelihood of a false positive.

3.1. Planet Candidates

WD 1202–232 b—Figure 1 shows the MIRI 15 μ m image of WD 1202–232 (top panels) before and after PSF subtraction of the WD and a nearby source, which is clearly visible at a separation of 1."11 \pm 0."04 at a position angle of $114^{\circ} \pm 2^{\circ}$ from north. These position measurements come from averaging the separation measured independently in each of the four filters. The absence of significant residuals in the PSF-subtracted images indicates the nearby source is not extended; all remaining flux is consistent with residuals after subtracting the star. Given a distance of 10.43 pc for WD 1202–232, if the planet is in a circular, face-on orbit, the star–planet separation is 11.47 au and the orbital period is 50 yr. During the host star's main-sequence lifetime, the planet's orbit would have been 5.3 au, assuming the planet moved out adiabatically after the host star mass-loss phase.

The candidate has a 15 μ m flux of $3.0 \pm 0.1 \, \mu$ Jy, consistent with a cool planetary-mass object at the distance of the star. The same source is seen in all four bands. Figure 2 shows the SED of the candidate planet around WD 1202–232 (left panel) along with the predicted SEDs from the Bern EXoplanet Cooling Curves with solar metallicity and no clouds (BEX; Linder et al. 2019a) for planet masses less than 2 $M_{\rm Jup}$ and the Burrows et al. (2003) models for higher mass planets. Using the total age of the star as the cooling time for the planet, this point source is consistent with the expected flux for a planetary-mass object of approximately 1–7 $M_{\rm Jup}$.

 $WD\ 2105-82\ b$ —The second candidate orbits WD 2105-82. MIRI imaging revealed a mid-infrared point source well separated from the WD at a separation of 2.14 ± 0.00 at a position angle of $200^{\circ}.4\pm0.00$ from north. Given the distance to the WD, if the candidate is in a face-on circular orbit, this translates to a star-planet separation of 34.62 au and a 243 yr Keplerian orbit. During the main-sequence phase, the planet would have been at 9.7 au. Figure 1 (lower panels) shows the candidate is a point source that is well subtracted in all filters using a PSF model created using a nearby bright star. A comparison with the BEX models (Linder et al. 2019b) shown in the right panel of Figure 2 indicates that the candidate planet's mass ranges from approximately 1 to $2M_{\rm Jup}$. In this case, the age of the WD is relatively well constrained, and the error in the planet mass is dominated by the photometric errors.

For both WD 1202–232 and WD 2105–82, the model SEDs in the four MIRI bands do not exactly match the observations. In general, the 5.6 and 7.7 μ m bands are brighter than expected compared to the 15 and 21 μ m bands. However, this is not sufficient evidence to rule out these candidates as planets. Planet models at these masses and temperatures are relatively unconstrained and they depend on the metallicity of the planet as well as the presence of clouds and haze in their atmospheres (Marley et al. 2021; Limbach et al. 2022). These unknowns can have a significant impact on the shape of the exoplanet's SED. Other, more exotic effects, such as tidally heated exomoons (Peters-Limbach & Turner 2013), could also cause the models to not match.

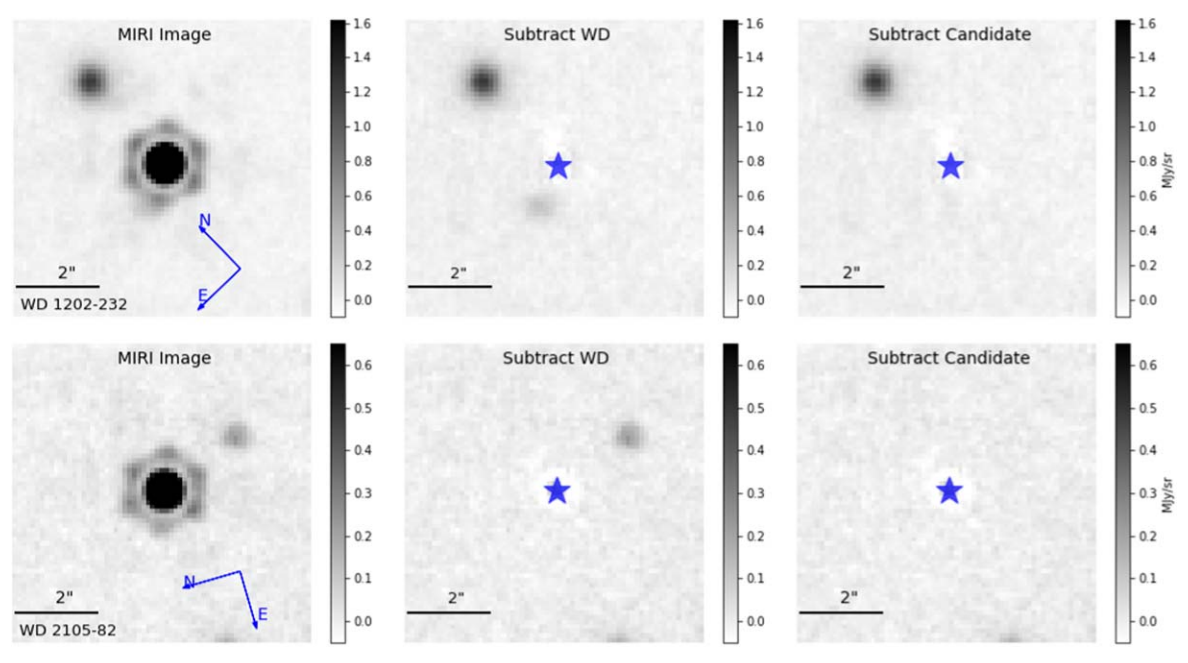


Figure 1. Image of each star and its candidate before and after subtracting a PSF modeled from a nearby bright star. Image cutouts are 65×65 pixels and the flux density units are in MJy per steradian. Left: original calibrated MIRI image cutout centered on the WD. The north and east directions are specified with blue arrows. Middle: the same image after scaling and subtracting the PSF centered on the WD. The location of the removed star is shown as a blue star. Right: the MIRI image after subtracting both the WD and the candidate using the same PSF. In both cases the candidate is removed cleanly, indicating it is point source in nature. Note that the bright object north of WD 1202-232 is a galaxy.

3.2. Potential False Positives

While the available observations are consistent with an orbiting exoplanet, we also consider other objects that would be consistent with the available evidence. The SED is inconsistent with a chance alignment with a typical main-sequence or evolved red giant star because even the coolest of these stars ($\sim 2000~\rm K$) would be brighter at 5 μ m than at 15 μ m (Husser et al. 2013) unless enshrouded in dust. A brown dwarf is possible, but if so, the flux of our candidates would place it farther away and unbound to the WD. Given the scarcity of isolated brown dwarf stars, this scenario is unlikely. An object in our own solar system, such as a trans-Neptunian object of the appropriate size, could appear as a very red point source, but likely would move by several pixels during the exposures. Additionally, both WDs lie at modest-to-high ecliptic latitudes (-21° and -60°) where the density of such objects is low.

The most likely false positive scenario is a distant galaxy. Galaxies have a variety of colors and can appear as a point source if sufficiently small or far away. While recent galaxy count studies with JWST can give a worst-case scenario to these odds (Ling et al. 2022; Wu et al. 2023), we can get a more precise feel for the likelihood of a false positive by counting the number of background sources in all four MIRI fields (9237 arcsec² per field) and determining the density of dim, red, point sources.

Following the same procedures outlined in Poulsen et al. (2023) we performed aperture photometry using the recommended aperture radii and background apertures across the entire field of view for both sets of observations. The core of each source was fit with a Gaussian to determine if its shape was consistent with a point source. We count red sources whose F1500W/F770W and F2100W/F1500W flux ratios are both greater than 1, as expected for a potential companion. We also limit the search to sources whose flux in the F1500W filter is less than $100 \,\mu \rm Jy$ because the BSL models find all planets

less than \approx 13 Jupiter masses at these target's distances and ages would be dimmer than this value. Counting across all four fields we find an average of five red point sources per MIRI field. The variation between fields range from three to eight dim, red objects per field, as one would expect based on counting error. For all fields, we use the average density of background sources to determine the rate of background sources, 0.54×10^{-3} sources per arcsecond². The larger the area of the search, the more likely we will include a background false positive. Within a 1."1 radius search (not including the inner 0."5 we could not search because of the target star), we found one dim, red candidate in all four fields, WD 1202–232 b. The odds of finding one object in four fields is inconsistent with the observed background density at a 2σ level at 2.18 or smaller. Each candidate, if it were the only candidate found, has a false alarm rate better than a 2σ result, 1/128 for WD 1202-232 and 1/29 for WD 2105-82. However, we actually found two candidates around four targets within 2"14. Using binomial statistics, finding two objects in four fields is inconsistent with the observed background density at a level of 1 in 3000 for a search radius of 2"2 or smaller. We conclude that both are exoplanet candidates and that it is very unlikely that both will be shown to be false positives.

4. Discussion

The best way to definitively confirm these candidate planets is to obtain a second epoch of the field with MIRI. The proper motion of WD 1202–232 is 230 mas yr⁻¹ and of WD 2105–82 is 463 mas yr⁻¹ (Gaia Collaboration et al. 2023). Because MIRI's pixels are 110 mas across (JDox 2016), this translates to a proper motion of 2 pixels yr⁻¹ for WD 1202–232 and 3.6 pixels yr⁻¹ for WD 2105–82. A second observation with JWST/MIRI could confirm common proper motion and the planetary nature of each candidate.

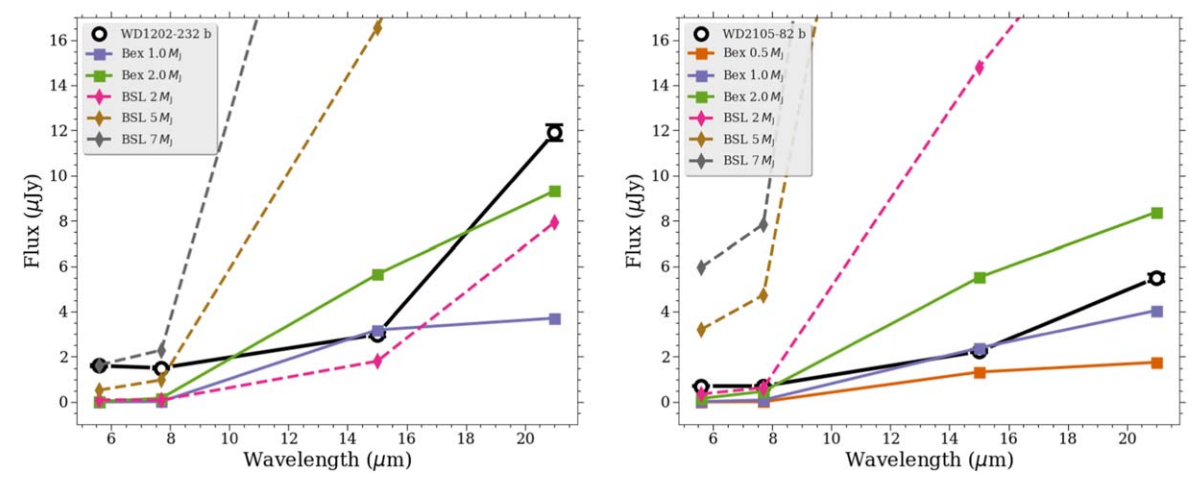


Figure 2. Photometric measurements for all four bands for both planet candidates (black circles) compared to low-mass planet models (squares) using the BEX (Linder et al. 2019a) and the models published by Burrows, Sudarsky, and Lunine (Burrows et al. 2003, hereafter BSL). WD 1202–232 b is shown on the left compared to models of 5.25 Gyr, and WD 2105–82 b is shown on the right compared to models at 1.6 Gyr for BEX and 1.0 Gyr for BSL (due to the available grid). While the photometry does not exactly match the models, the flux in all four bands is consistent with a giant-mass planet at the age of the WD and shows increasing flux with wavelength.

Current models for what drives the pollution on these WDs indicate that many could have observable planetary companions. Veras (2021) lists a variety of models that seek to explain the source of WD metal pollution. While all invoke the destruction of some kind of minor planet (a comet or asteroid) as a direct explanation of the pollution, models differ in how to transport those minor planets from beyond 3 au to the Roche limit where they are disrupted. The standard model of Debes & Sigurdsson (2002), Frewen & Hansen (2014), and others invoke changes in the orbit of a large planet (either due to stellar mass-loss in the asymptotic giant-branch stage, or planet-planet scattering) to drive orbital instability in the minor planets (the so-called very late heavy bombardment). If that theory is correct, we expect all such polluted stars to host a giant planet ($\gtrsim 0.1 M_{\text{Jup}}$, roughly twice Neptune's mass). While MIRI images are not sensitive to the smaller giant planets, it is likely to be sensitive to planets above $\approx 1 M_{\text{Jup}}$ as shown by Poulsen et al. (2023) for similar observations. If the mass distribution for giant long-period planets reported by Fernandes et al. (2019) is accurate, JWST observations should be sensitive to approximately a third of the expected giant companions. Failure to find any planets orbiting four WDs would start to shift the burden of evidence strongly in favor of models such as Caiazzo & Heyl (2017) and Veras & Rosengren (2023) that invoke much smaller planets to explain the accretion of materials onto WDs. A future paper will discuss detection limits and any widely separated candidates for the entire sample of MIRI observations.

If confirmed, these two planet candidates provide concrete observational evidence that outer giant planets like Jupiter survive the evolution of low-mass stars. Their existence would support the dominant paradigm for the planet–pollution connection, arguing that wide-orbit giant planets are ubiquitous. Confirmation would also support the indirect evidence that 25%–50% of WDs host large planets (as inferred from the fraction of metal-polluted WDs; Koester et al. 2014). This would mean that the occurrence rate of giants around WD progenitors (B–F type stars) is also high. Confirmation would support the conclusions of ground-based direct imaging surveys of young stars (Nielsen et al. 2019; Vigan et al. 2021) that B and A stars have a higher fraction of giant

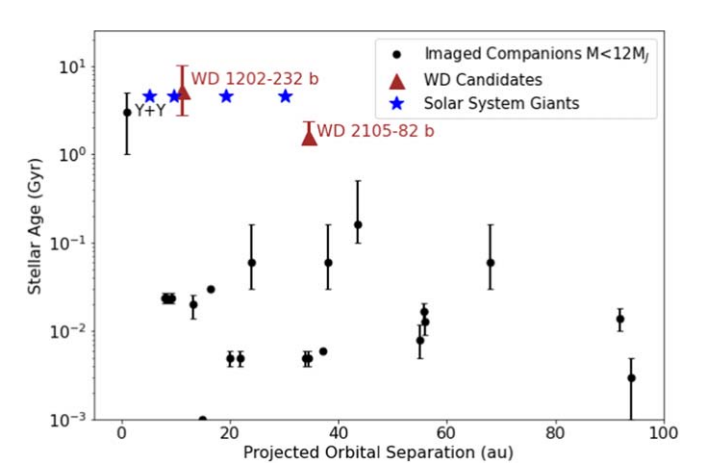


Figure 3. Projected orbital separation vs. the age of the star the companion is orbiting for directly imaged planets less than 12 $M_{\rm Jup}$ (black circles). The two WD planet candidates are presented with brown triangles. The solar system giant planets are shown as blue stars. The candidates are significantly older than all previously reported directly imaged, low-mass companions, except the Y+Y dwarf binary system (WISE J033605.05-014350.4) recently found using JWST by Calissendorff et al. (2023).

planets than solar-type stars. The confirmation of these planets is not, however, sufficient to fully validate that large-mass giant planets are the drivers of accretion without further observations. Only by surveying more nearby WDs, both with and without metal lines in the atmosphere, can we determine whether large giant planets are more common around metal-polluted WDs. A first step toward such a survey will be undertaken by JWST starting in Cycle 2 through the MEAD (GO 3964) and MEOW (GO 4403) survey programs, which may be sensitive to the brighter, more massive, giant planets.

These candidates would represent the oldest directly imaged planets outside our own solar system, and in many ways are more like the planets in our outer solar system than ever discovered before. Figure 3 shows a comparison with confirmed planets and brown dwarfs compiled by the NASA Exoplanet Science Institute (2020). These candidate planets are likely only a few times the mass of Jupiter and their separation during the main sequence (5.3 and 9.7 au) is similar to the

orbits of Jupiter and Saturn in our own solar system. Furthermore, the ages of these planets, and hence their temperatures, are more similar to the 4.6 billion yr old age of our own solar system than previously directly imaged exoplanets around much younger stars (e.g., Nielsen et al. 2019). Thermal emission from a cool, middle-aged exoplanet provides critical constraints on atmospheric properties that also fold back into a greater understanding of the cold giant planets in our solar system. Direct detection of the thermal emission from cold ($T_{\rm eff}$ < 200 K) planets is particularly important for understanding the presence or absence of water clouds, similar to that seen for Jupiter (Morley et al. 2014; Marley et al. 2021). The impact of clouds on exoplanet emission could be significant; cloudy planets lose their prominent emission at $4.5 \mu m$, while colder, cloudless planets may be fainter at wavelengths beyond 10 μ m (Limbach et al. 2022).

5. Conclusions

We have found evidence of two giant planets orbiting two different DAZs using broadband mid-infrared imaging with JWST's MIRI. The sensitivity and resolution of MIRI along with the light-gathering power of JWST have made it possible to image previously unseen middle-aged giant planets orbiting nearby stars, all without a coronagraph. The most likely false positive scenario is a distant red galaxy; however, background source counts indicate finding such a galaxy so close to both WDs at 15 μ m is highly unlikely. If confirmed using common proper motion, these giant planets will represent the first directly imaged planets that are similar in age, mass, and orbital separation as the giant planets in our own solar system. Future spectroscopy and multiband imaging of these systems may be possible with JWST, which would improve the observational constraints on the physics and variety of cool giant planet models.

Acknowledgments

The authors would like to thank the anonymous referee for providing very useful comments that improved this paper. This work is based on observations made with the NASA/ESA/CSA James Webb Space Telescope. The data were obtained from the Mikulski Archive for Space Telescopes at the Space Telescope Science Institute, which is operated by the Association of Universities for Research in Astronomy, Inc., under NASA contract NAS 5-03127 for JWST. Support for program number 1911 was provided through a grant from the STScI under NASA contract NAS5-03127. M.K. acknowledges support by the NSF under grant AST-2205736 and NASA under grant 80NSSC22K0479.

Software: Astropy (The Astropy Collaboration et al. 2013), Matplotlib (Hunter 2007).

ORCID iDs

Susan E. Mullally https://orcid.org/0000-0001-7106-4683
John Debes https://orcid.org/0000-0002-1783-8817
Misty Cracraft https://orcid.org/0000-0002-7698-3002
Fergal Mullally https://orcid.org/0009-0004-7656-2402
Sabrina Poulsen https://orcid.org/0009-0008-7425-8609
Loic Albert https://orcid.org/0000-0003-0475-9375
Katherine Thibault https://orcid.org/0009-0004-6806-1675
William T. Reach https://orcid.org/0000-0001-8362-4094
J. J. Hermes https://orcid.org/0000-0001-5941-2286

```
Thomas Barclay https://orcid.org/0000-0001-7139-2724 Mukremin Kilic https://orcid.org/0000-0001-6098-2235 Elisa V. Quintana https://orcid.org/0000-0003-1309-2904
```

References

```
Alcock, C., Fristrom, C. C., & Siegelman, R. 1986, ApJ, 302, 462
Bédard, A., Bergeron, P., Brassard, P., & Fontaine, G. 2020, ApJ, 901, 93
Blackman, J. W., Beaulieu, J. P., Bennett, D. P., et al. 2021, Natur, 598, 272
Brandner, W., Zinnecker, H., & Kopytova, T. 2021, MNRAS, 500, 3920
Burleigh, M. R., Clarke, F. J., & Hodgkin, S. T. 2002, MNRAS, 331, L41
Burleigh, M. R., Clarke, F. J., Hogan, E., et al. 2008, MNRAS, 386, L5
Burrows, A., Sudarsky, D., & Lunine, J. I. 2003, ApJ, 596, 587
Caiazzo, I., & Heyl, J. S. 2017, MNRAS, 469, 2750
Calissendorff, P., De Furio, M., Meyer, M., et al. 2023, ApJL, 947, L30
Choi, J., Dotter, A., Conroy, C., et al. 2016, ApJ, 823, 102
Cummings, J. D., Kalirai, J. S., Tremblay, P.-E., Ramirez-Ruiz, E., & Choi, J.
   2018, ApJ, 866, 21
Debes, J. H., & Sigurdsson, S. 2002, ApJ, 572, 556
Debes, J. H., Sigurdsson, S., & Woodgate, B. E. 2005a, AJ, 130, 1221
Debes, J. H., Sigurdsson, S., & Woodgate, B. E. 2005b, ApJ, 633, 1168
Debes, J. H., Walsh, K. J., & Stark, C. 2012, ApJ, 747, 148
Farihi, J., Becklin, E. E., & Zuckerman, B. 2008, ApJ, 681, 1470
Fernandes, R. B., Mulders, G. D., Pascucci, I., Mordasini, C., &
   Emsenhuber, A. 2019, ApJ, 874, 81
Fontaine, G., Brassard, P., & Bergeron, P. 2001, PASP, 113, 409
Frewen, S. F. N., & Hansen, B. M. S. 2014, MNRAS, 439, 2442
Gaia Collaboration, Vallenari, A., Brown, A. G. A., et al. 2023, A&A, 674, A1
Gänsicke, Boris T., Schreiber, Matthias R., Toloza, Odette, et al. 2019, Natur,
Gentile Fusillo, N. P., Tremblay, P. E., Jordan, S., et al. 2018, MNRAS,
   473, 3693
Gianninas, A., Bergeron, P., & Ruiz, M. T. 2011, ApJ, 743, 138
Heintz, T. M., Hermes, J. J., El-Badry, K., et al. 2022, ApJ, 934, 148
Hogan, E., Burleigh, M. R., & Clarke, F. J. 2009, MNRAS, 396, 2074
Hunter, J. D. 2007, CSE, 9, 90
Husser, T. O., Wende-von Berg, S., Dreizler, S., et al. 2013, A&A, 553, A6
JDox 2016, JWST User Documentation (JDox), JWST User Documentation
Jura, M. 2003, ApJL, 584, L91
Kiman, R. 2022, rkiman/wdwarfdate: First release of wdwarfdate, v1.0.0,
   Zenodo, doi:10.5281/zenodo.6633759
Koester, D. 2009, A&A, 498, 517
Koester, D., Gänsicke, B. T., & Farihi, J. 2014, A&A, 566, A34
Landstreet, J. D., Bagnulo, S., Valyavin, G. G., et al. 2012, A&A, 545, A30
Limbach, M. A., Vanderburg, A., Stevenson, K. B., et al. 2022, MNRAS,
   517, 2622
Linder, E. F., Mordasini, C., Mollière, P., et al. 2019a, A&A, 623, A85
Linder, E. F., Mordasini, C., Mollière, P., et al. 2019b, A&A, 623, A85
Ling, C.-T., Kim, S. J., Wu, C. K. W., et al. 2022, MNRAS, 517, 853
Luhman, K. L., Burgasser, A. J., Labbé, I., et al. 2012, ApJ, 744, 135
Marley, M. S., Saumon, D., Visscher, C., et al. 2021, ApJ, 920, 85
Melis, C., Farihi, J., Dufour, P., et al. 2011, ApJ, 732, 90
Morley, C. V., Marley, M. S., Fortney, J. J., et al. 2014, ApJ, 787, 78
Mullally, F., Kilic, M., Reach, W. T., et al. 2007, ApJS, 171, 206
Mullally, S. E., Mullally, F., Albert, L., et al. 2021, A Search for the Giant
   Planets that Drive White Dwarf Accretion, JWST Proposal. Cycle 1,
Mustill, A. J., & Villaver, E. 2012, ApJ, 761, 121
NASA Exoplanet Science Institute 2020, Planetary Systems Table, NASA
   Exoplanet Archive, IPAC doi:10.26133/NEA12
Nielsen, E. L., De Rosa, R. J., Macintosh, B., et al. 2019, AJ, 158, 13
Peters-Limbach, M. A., & Turner, E. L. 2013, ApJ, 769, 98
Poulsen, S., Debes, J., Cracraft, M., et al. 2023, arXiv:2311.14165
Soker, N., Livio, M., & Harpaz, A. 1984, MNRAS, 210, 189
Subasavage, J. P., Jao, W.-C., Henry, T. J., et al. 2017, AJ, 154, 32
The Astropy Collaboration, Robitaille, T. P., Tollerud, E. J., et al. 2013, A&A,
   558, A33
Tremblay, P. E., Ludwig, H. G., Steffen, M., & Freytag, B. 2013, A&A,
Trierweiler, I. L., Doyle, A. E., & Young, E. D. 2023, PSJ, 4, 136
van Sluijs, L., & Van Eylen, V. 2018, MNRAS, 474, 4603
Vanderburg, A., Rappaport, S. A., Xu, S., et al. 2020, Natur, 585, 363
Veras, D. 2021, Oxford Research Encyclopedia of Planetary Science (Oxford:
   Oxford Univ. Press), 1
```

Veras, D., & Rosengren, A. J. 2023, MNRAS, 519, 6257 Vigan, A., Fontanive, C., Meyer, M., et al. 2021, A&A, 651, A72 Wolszczan, A., & Frail, D. A. 1992, Natur, 355, 145

Wolthoff, V., Reffert, S., Quirrenbach, A., et al. 2022, A&A, 661, A63 Wu, C. K. W., Ling, C.-T., Goto, T., et al. 2023, MNRAS, 523, 5187 Xu, S., Dufour, P., Klein, B., et al. 2019, AJ, 158, 242